Open access • Journal Article • DOI:10.1016/J.ECSS.2016.03.027

Coastal flood protection by a combined nature-based and engineering approach: modeling the effects of marsh geometry and surrounding dikes — Source link

J. Stark, Yves Plancke, Stefaan Ides, P. Meire ...+1 more authors

Institutions: University of Antwerp

Published on: 20 Jun 2016 - Estuarine Coastal and Shelf Science (Academic Press)

Topics: Marsh, Coastal flood, Storm surge and Wetland

Coastal flood protection by a combined nature-based and engineering approach : modeling the effects of marsh geometry and surrounding dikes

Reference:

Stark Jeroen, Plancke Yves, Ides Stefaan, Meire Patrick, Temmerman Stijn.- Coastal flood protection by a combined nature-based and engineering approach : modeling the effects of marsh geometry and surrounding dikes
Estuarine, coastal and shelf science - ISSN 0272-7714 - 175(2016), p. 34-45
Full text (Publishers DOI): http://dx.doi.org/doi:10.1016/j.ecss.2016.03.027
To cite this reference: http://hdl.handle.net/10067/1327450151162165141

Stark J., Plancke Y., Ides S., Meire P., Temmerman S., Coastal flood protection by a combined nature-based and engineering approach: Modeling the effects of marsh geometry and surrounding dikes. Estuarine, Coastal and Shelf Science, 175, pp. 34-45, doi: 10.1016/j.ecss.2016.03.027

Corresponding author:
Jeroen Stark
University of Antwerp - Ecosystem Management Research Group
Universiteitsplein 1 C0.31 | BE-2610 Antwerpen
jeroen.stark@uantwerpen.be
+32 (0) 3 265 2759 / +32487442139

Abstract

As ecosystem-based adaptation to global change is gaining ground, strategies to protect coastal and estuarine areas from increasing flood hazards are starting to consist of natural tidal wetland conservation and restoration in addition to conventional coastal defense structures. In this study, the capacity of tidal wetlands to locally attenuate peak water levels during storm tides is analyzed using a two-dimensional hydrodynamic model (TELEMAC2D) for a 3000 ha intertidal marsh (SW Netherlands). Model results indicate that peak water level reduction largely varies between individual flooding events and between different locations in the marsh. Model scenarios with variable dike positions show that attenuation rates can be minimized by blockage and set up of water levels against dikes or other structures confining the marsh size. This blockage only affects peak water level attenuation across wetlands if the duration of the flood wave is long compared to the marsh size. A minimum marsh width of 6 to 10 km is required to completely avoid blockage effects for the storm tidal cases assessed in this study. If blockage does not affect flood wave propagation, variations in attenuation rates between different locations in the marsh and between

tides with varying high water levels can be explained with a single relationship based on the ratio between the water volume on the marsh platform and the total water volume on the platform and in the channels. Attenuation starts to occur when this ratio exceeds 0.2-0.4 and increases from there on up to a maximum of 29 cm/km for a ratio of about 0.85. Furthermore, model scenarios with varying marsh channel depth show that marsh scale attenuation rates increase by up to 4 cm/km if the channel elevation is raised by 0.7 m on average. Conversely, marsh scale attenuation rates decrease by up to 2 cm/km for scenarios in which the channels are lowered by 0.9 m on average. The marsh platform elevation has little effect on the maximum attenuation, but it determines which tides are attenuated. In particular, only overmarsh tides that inundate the platform are attenuated, while undermarsh tides that only flood the marsh channels are not attenuated or even amplified. These findings may assist coastal communities and managers in the optimization of the coastal defense function of tidal wetlands in combination with dikes.

1. Introduction

Ecosystem- or nature-based adaptation is an increasingly adopted strategy to cope with natural hazards that may increase with global change (e.g., Barbier, 2014; Hinkel et al., 2014; Jones et al., 2012; Kundzewicz et al., 2014). For coasts and estuaries, which are increasingly exposed to flood hazards from sea level rise and storm surges (e.g., Nicholls and Cazenave, 2010; Woodruff et al., 2013), the potential of tidal wetlands, including mangroves and marshes, for the reduction of flood risks is increasingly recognized around the world (e.g., Gedan et al., 2010; Shepard et al., 2011; Temmerman et al., 2013). In particular, there is growing interest to combine nature-based coastal defense functions of tidal wetlands with engineered coastal defense structures such as dikes (Cheong et al., 2013; Sutton-Grier et al., 2015; Temmerman and Kirwan, 2015). Besides the ecological functions of wetlands, these ecosystems may also contribute to coastal protection as they reduce the height of wind waves (e.g., Möller et al., 2014, 1999) and storm surges (e.g., Krauss et al., 2009; Lovelace, 1994; McGee et al., 2006; Wamsley et al., 2010) through additional flow resistance exerted by the wetland vegetation and wetland geomorphology. Moreover, wetlands may also reduce storm surges by increasing the storage area along estuaries or tidal rivers (e.g., Smolders et al., 2015). The focus of this study is however on the potential of tidal marshes to reduce storm surges locally within and behind the marsh area.

The capacity of tidal marshes and mangroves to attenuate storm surges is typically expressed as the reduction of high water levels (HWLs) per distance that the surge has travelled through a tidal wetland, i.e. the storm surge attenuation rate in cm/km. So far, existing insights on storm surge reduction rates in marshes are limited and based on scarce field studies, which were mainly conducted for one or a few specific hurricane or storm surge events (see McIvor et al. 2012 or Stark et al. 2015 for a more detailed literature review of observed storm surge attenuation rates).

Additional insights come from hydrodynamic modeling studies, which are mostly hind-casts of specific hurricane events (e.g., Wamsley et al., 2010; Zhang et al., 2012) or consider marsh geometry in a highly schematized way (e.g., Loder et al., 2009; Temmerman et al., 2012). Peak water level reduction rates ranging from 4 to 25 cm/km are observed in previous field studies. The high variety in observed attenuation rates suggests a strong dependency on the local marsh geomorphology and on the specific hydrodynamic forcing conditions. Besides, the morphological development of marshes may lead to variations of the attenuation capacity over time.

Numerical modeling studies have shown that storm surge attenuation is dependent on event-specific variables such as storm track and duration (Hu et al., 2015; Rego and Li, 2009; Resio and Westerink, 2008; Sheng et al., 2012; Wamsley et al., 2010; Weisberg and Zheng, 2006; Zhang et al., 2012). In particular, Resio and Westerink (2008) explained that attenuation rates decrease for larger storm surges and longer inundation events, because the surge has more time to fill up the entire marsh storage area. Wamsley et al. (2009) drew a similar conclusion to explain amplification of HWLs over marsh sections where levees precluded the surge to move further inland. Lower attenuation rates for extremely high inundation events were also observed during in-situ measurements by Stark et al. (2015), who attributed this to limitations in storage area, vegetation submergence and the decreasing effect of bottom friction on the marsh.

Numerical studies on the effect of channel density and channel geometry on storm surge reduction show that marshes with more and wider or deeper channels lead to lower attenuation rates than marshes which are dissected by fewer or smaller channels (e.g., Loder et al., 2009; Temmerman et al., 2012). Similar tendencies were found in field observations (Krauss et al., 2009; Stark et al., 2015; Van der Molen, 1997), where the highest attenuation rates were observed along narrow or shallow channel transects. The effect of the elevation of the marsh platform on surge development over a schematized continuous marsh has been assessed numerically for hurricane induced surges (Loder et al., 2009; Wamsley et al., 2010) and with field observations for the propagation of regular tides and storm tides (Stark et al., 2015), which indicate that attenuation only occurs for a specific range of HWLs above the platform elevation. A variety of numerical studies showed that flood wave attenuation is significantly influenced by additional surface roughness due to marsh vegetation cover (e.g., Hu et al., 2015; Loder et al., 2009; Sheng et al., 2012; Temmerman et al., 2012; Zhang et al., 2012). This would suggest that the extent of the vegetated marsh platform relative to the extent of the channels dissecting the platform determines the rate of attenuation. However, no geometrical measure or parameter is found yet in which the effects of variations in marsh geometry are combined with variations in flood wave height, and based on which the storm surge attenuation capacity of tidal wetlands can be predicted. Furthermore, the effect of the position of dikes confining the marsh size on flood level reduction is still poorly studied. To our knowledge, there are no existing studies in which the effect of marsh size is quantified by comparing flood level reduction rates for variable dike positions. As the interest of coastal managers for 'hybrid' coastal defense strategies based on a combination of engineering and nature-based solutions is growing (e.g. Sutton-Grier et al., 2015; Temmerman and Kirwan, 2015), insights on the potential for flood level reduction provided by coastal and estuarine marshes and how they interact with conventional coastal defense structures such as dikes need to be improved.

In this study, we assess the effect of the geometrical properties of an intertidal marsh and the position of the dikes surrounding the marsh on storm surge reduction rates within the marsh itself and consequently at the dikes behind the marsh. A hydrodynamic model is set up for a large tidal marsh including its complex channel network. First the model is calibrated and validated with water level measurements of several spring neap cycles and two storm tides. Scenario analyses are then performed, in which artificial changes are made to the marsh geomorphology and position of dikes surrounding the marsh. In particular, these scenarios focus on the effect of variations in dike position (affecting marsh size), marsh platform elevation and channel depth on the rates of HWL reduction within the marsh. Ultimately, we derive a single parameter based on the model simulations that links the spatial variations (depending on the marsh geometry) and temporal variations (depending on the height of the flood event) to the HWL reduction rate.

2. Methods

2.1 Study area

The studied marsh is the 'Verdronken Land van Saeftinghe' (in the following: 'Saeftinghe'), a 3000 ha brackish intertidal marsh along the Western Scheldt estuary (SW Netherlands) (Fig. 1). A semi-diurnal macrotidal regime induces HWLs at the study area between 2.18 m and 3.15 m above NAP (the Dutch ordnance level, close to mean sea level) for neap and spring tides respectively. The tidal range varies between 4.02 m and 5.57 m. The Saeftinghe marsh geometry is characterized by three main channels dissecting the marsh platform, called Speelmansgat in the west, IJskelder in the middle and Hondegat in the east (in this study referred to by S-, Y- and H-channels) (Fig. 2). The three main channels are several hundreds of meters wide at the marsh edge and branch in the landward direction into a complex network of smaller channels. The channels dissecting the marsh are intertidal, implying that they fall dry during low tide. On the marsh platform itself, the most abundant vegetation types are *Elymus athericus* and *Scirpus maritimus*. Other species that occur are *Puccinellia maritima*, *Spartina anglica*, *Aster tripolium* and scattered patches of *Phragmites australis*. Vegetation canopy height depends on the local species composition and may be estimated as around 0.42 m on average (Vandenbruwaene et al., 2015). An artificial dam that is only flooded during high storm tides is present within the eastern part of the marsh (Fig. 2b). Wang and Temmerman (2013) presented a historical analysis of the geomorphological and vegetation development of the Saeftinghe marsh from the 1930s until 2004. During this period, the vegetated part of the marsh increased from 50% to 70% of the total area. The mean elevation of Saeftinghe increased from 1.13 m to 2.30 m above NAP, while mean high water levels increased from 2.36 m to 2.76 m. Accordingly, the mean elevation of the bare flats and intertidal channels increased from NAP +0.56 m in 1931 to NAP +0.90 m NAP in 2004, while the mean elevation of the vegetated platform increased even more from NAP +1.92 m to 2.81 m in 2004. This latter value is used for the analyses in this study.

2.2 Hydrodynamic model

The numerical model used in this study is set up with TELEMAC-2D (version 6.3), a widely used hydrodynamic modeling system that is part of the TELEMAC-MASCARET modeling suite and contains the relevant physical processes with respect to tidal wave propagation in estuaries (Hervouet, 2007). This two-dimensional hydrodynamic model solves the depth-averaged Navier-Stokes equations for continuity (Eq. 1) and momentum (Eq. 2-3) simultaneously:

(1) $$\frac{\delta U}{\delta x} + \frac{\delta V}{\delta y} = S_h$$

(2) $$\frac{\delta U}{\delta t} + U\frac{\delta U}{\delta x} + V\frac{\delta U}{\delta y} = -g\frac{\delta h}{\delta x} + \nu\nabla U + S_x$$

(3) $$\frac{\delta V}{\delta t} + U\frac{\delta V}{\delta x} + V\frac{\delta V}{\delta y} = -g\frac{\delta h}{\delta y} + \nu\nabla V + S_y$$

in which U and V (m/s) are the flow velocity components in Cartesian coordinates, S_h (m/s) is a source or sink term for fluid, g (m/s^2) is the gravity acceleration, h (m) is the water depth, ν (m^2/s) is a momentum diffusivity coefficient and S_x and S_y (m^2/s) are sources or sinks (such as wind force, Coriolis force and bottom friction) of momentum in the dynamic equations. In our case, the viscosity coefficient ν which represents both the molecular as well as the turbulent viscosity is set constant for the entire model domain. For more detailed information on the TELEMAC-2D model we refer to (Hervouet, 2007) and the TELEMAC-2D user manual (see: http://wiki.opentelemac.org/).

2.2.1 Model description

The model mesh used in this study is adopted from Smolders et al. (2015) who calibrated and validated a tidal model (including storm tides) for the Scheldt estuary from its mouth in the North Sea up to its most upstream tidal boundaries (Fig. 1). The mesh size ranges from approximately 10-50 m in the most upstream tributaries up to about 150-200 m in the most downstream part of the estuary. For this study, the model is locally refined to a mesh size of 6-20 m at the Saeftinghe study area to include the complex marsh geomorphology as good as possible and to represent the locations of the water level measurements more accurately (see Fig. 2b for these locations). The refinement increases the number of nodes to 130175. The extensive network of channels and creeks that dissect the marsh platform is included in the mesh by forcing the mesh to follow the marsh channel network to the extent possible. This channel network has been extracted from a Lidar-based Digital Elevation Model (DEM) with a resolution of 2x2 m using GIS-software.

Bathymetric and topographic data from 2009 to 2011 are used to implement the bathymetry of the estuary, its tributaries and the Saeftinghe geomorphology in the model. The effect of vegetation on tidal propagation through the marsh is included by assigning higher bottom friction coefficients to vegetated areas than to non-vegetated areas. Vegetation maps (Huijs, 1995; Reitsma, 2006) are used to distinguish vegetated from non-vegetated areas. All types of vegetation are wrapped into a single Manning bottom friction coefficient because the spatial distribution of the vegetation types is too scattered to distinguish large areas with different vegetation characteristics on the scale we are modeling. Moreover, the dominant vegetation species have rather similar characteristics (i.e., flexible wetland grass types). The value for the overall bottom friction coefficient representing the combined effect of all types of marsh vegetation is derived by calibration. Drawback of implementing vegetation by constant Manning friction coefficients is that the depth-dependent effect of the vegetation (i.e., submerged versus emerged) on the flow is not incorporated (Baptist et al., 2007). However, previous modeling studies on storm surge propagation in wetlands have shown that reasonable results can be obtained while using constant or depth-independent Manning coefficients (e.g., Liu et al., 2013; Wamsley et al., 2009; Zhang et al., 2012).

The North Sea boundary of the model is forced with tidal water levels obtained from nearby tidal stations in the North Sea and along the coast. The upstream boundaries of the tributaries are closed, as the influence of the small discharges from these tributaries (i.e., on average 118 m^3/s over 2013 as reported by Vanlierde et al., 2014) can be considered negligible compared to the tidal forcing at the study area. Wind effects are not taken into account in the model, implying that the wind set up that develops locally in the estuary or over the marsh area is not simulated. However, storm surges in the Western Scheldt are mainly generated by wind and atmospheric pressure effects on the North Sea, which is outside the model domain. Surge generation in the estuary itself is relatively small due to shorter fetch lengths and relatively low water depths. In the model, storm surges are included as boundary conditions at the North Sea model boundary.

2.2.2 Model calibration and validation

The hydrodynamic model of the Western Scheldt, without considering the Saeftinghe study area, is calibrated on tidal water levels by implementing zones with different Manning's bottom friction coefficients n, varying from 0.010 to 0.026 (Smolders et al., 2015). For this particular study, the performance of the model was optimized further for tidal stations near the Saeftinghe marsh by slightly tuning bottom friction coefficients. The model performance on estuary scale is assessed by forcing a spring-neap cycle (30/8/2013-27/9/2013) at the seaward water level boundary. Mean errors (ME), root mean square errors (RMSE) and mean absolute errors (MAE) are calculated for simulated against observed water levels at several tidal stations from the estuary mouth near Vlissingen up to Antwerp (see Fig. 1 for locations of the tidal stations). The mean error is also calculated for the HWLs specifically (ME_{HWL}), just as the phase difference of the HWLs ($\Delta\varphi_{\text{-HWL}}$).

In this study, we focus specifically on the model performance with respect to the representation of tidal wave propagation and storm surge attenuation within the Saeftinghe marsh. In-situ water level observations by Stark et al. (2015) are used for the calibration of the model in the marsh study area itself. These water level measurements were conducted in and around the 4 km Hondegat channel in the Saeftinghe marsh at the locations shown in Fig. 2b and include several spring-to-neap cycles and two storm tides, the highest of which induced HWLs at tidal stations near the study area with an exceedance probability of 1/5 to 1/10 y^{-1}. Calibration of the model part representing the Saeftinghe marsh is done by tuning Manning's bottom friction coefficients n_f and n_v for unvegetated and vegetated parts of the marsh respectively. In addition, the spatially and temporally constant velocity diffusivity coefficient ν is tuned to optimize the representation of tidal propagation through the marsh channels. Values used in the calibration are between 0.01 and 0.03 for the bottom friction on the unvegetated tidal flats and channels, between 0.04 and 0.20 for the bottom friction coefficient on the vegetated marsh platform and 10^{-4} to 2.0 for the velocity diffusivity coefficient. Best results are obtained with $n_f = 0.01$, $n_v = 0.08$ and $\nu = 0.5$. The model performance in Saeftinghe is assessed with a comparison between simulated and observed water levels (i.e., 30/8/2013-27/9/2013 & 1/12/2013-15/12/2013) for which the ME, MAE and RMSE are calculated. In addition, ME_{HWL} and $\Delta\varphi_{\text{-HWL}}$ are calculated as well. Finally, we compare simulated attenuation rates with observed rates for a variety of HWLs.

2.3 Model scenarios

Model scenarios are set up in which the marsh geometry is altered to assess the influence of marsh scale geomorphology on the attenuation of peak water levels (Table 1). Although marsh platform elevation and marsh channel elevation are not independent, they are independently lowered or raised in the model scenarios in order to gain fundamental insights in their individual impacts on storm surge attenuation. Artificial elevation changes within the tidal frame are applied to the elevation of the marsh platform (±0.4 m) and channels (±0.9 m). To prevent the local platform elevation from becoming lower than adjacent channels, the elevation of the vegetated platform was restricted to a minimum of NAP +2.4 m, while the local elevation of the bare channels was restricted to a maximum of NAP +2.4 m to ensure that the channel elevation does not rise above the surrounding platform. This leads to scenarios in which the channel elevation is lowered by 0.9 m on average (Run 3) or raised by 0.7 m on average (Run 4) and in which the platform elevation is either raised or lowered by 0.4 m on average (Run 5 & Run 6). Furthermore, simulations are performed in which the marsh size is increased by repositioning the dike on the south side of Saeftinghe to a more landward position and hence extending the marsh width by approximately 1 km (Run 1) and 5 km (Run 2). The extended part of the marsh is schematized as a continuous vegetated marsh or grassland (n_v = 0.08) at an elevation of NAP +3.0 m (i.e., approximately the mean platform elevation of the study area) and without any channels dissecting the platform. These simulations are used to assess the effect of marsh size (i.e. storage area on the platform) and whether it is a limiting factor for storm surge attenuation in case of larger surge events. All model simulations consist of a series of regular tides and storm tides that is set up by manually altering the amplitude of a regular tide and of the measured storm tide in December

2013 (Fig. 3). Attenuation and amplification rates are calculated over the S-, Y- and H channels (see Fig. 2) for all geomorphological scenarios.

Table 1. Overview of model scenarios.

Simulation	Description of scenario
Run 0	Reference scenario with 2011 bathymetry of Saeftinghe
Run 1	Marsh platform extended / Dike behind marsh moved landward by 1 km
Run 2	Marsh platform extended / Dike behind marsh moved landward by 5 km
Run 3	Channel elevation lowered by 0.9 m
Run 4	Channel elevation increased by 0.7 m
Run 5	Platform elevation lowered by 0.4 m
Run 6	Platform elevation increased by 0.4 m

2.4 Analysis of relations between attenuation rates and marsh geometry

The three main channels of the marsh are divided in shorter transects to analyze the relation between the spatially varying marsh geometry and attenuation rates more specifically. In particular, we attempt to relate HWL reduction rates over shorter channel sections to local geometrical properties of the marsh. Local attenuation rates are calculated for the simulation in which the platform area is extended by 5 km (Run 2 in Table 1) to exclude the effects of water level setup against the dikes and hence isolate the effects of marsh geomorphology on tidal attenuation or amplification. The analysis is only done for the S- and Y-transects as storm surge propagation along the H-transect for the highest HWLs is affected by water entering the marsh over the low man-made dam in the eastern part of the marsh (see Fig. 2). This makes the analysis of storm surge propagation along the H-transect more complex. To avoid miscellaneous results, the S5-S6 section is also excluded, because the direction of the flood wave propagation (i.e.

direction of the water level gradient) for high overmarsh tides differs from the orientation of this channel section. Only overmarsh tides with HWLs of at least 0.4 m above mean platform elevation are included in the analysis. For these higher tides, large scale sheet flow over the marsh surface occurs in the model simulations, reducing the influence of flow routing through the channels on water level variations (Temmerman et al., 2005a, 2005b). Attenuation rates are calculated as the HWL difference along each section (i.e., S1-S2-..-S5 and Y1-Y2-..-Y5 sections) divided by the difference in distance from the front edge of the marsh between the beginning and end of each section (calculated as the bird's fly distance between the marsh edge and the along-channel locations). Various geometrical parameters, which relate the marsh geometry to the amount of friction exerted on the propagating storm tides, are computed for each section in an attempt to relate them to simulated attenuation rates. Geometrical parameters include mean channel width, mean cross-sectional area of the channel, mean channel depth, maximum channel depth, width and depth convergence length scales of the channel, mean platform elevation and an estimate for the ratio (α_A) between the vegetated surface area (A_{pl}) and the total surface area ($A_{ch}+A_{pl}$) along each channel section. These vegetated (A_{pl}) and non-vegetated (A_{ch}) surface areas are derived from vegetation maps for a 500 m wide band on both sides along the thalweg (corresponding to the minimum distance needed to include the marsh platform along the widest of the investigated channel sections) with GIS software (ArcGIS, version 10.1). This parameter is considered as a proxy for the ratio between marsh platform width and the total width of the channel and the platform, which Stark et al. (2015) adopted from Van Rijn (2011) to explain differences in attenuation rates between marsh channels with varying geometry. Ultimately, attenuation rates are for each tide compared to the ratio between the water volume above the platform and the total water volume (i.e. above the channels and above the platform) present in each section ($\alpha_v = V_{pl}/(V_{ch}+V_{pl})$).

3. Results

3.1. Model Validation

To validate the model performance on the estuary scale, observed and modeled series of water levels are compared in Table 2, which also contains the mean error and average phase difference between the observed and modeled HWLs. Average phase differences near the study area (i.e. Bath and Baalhoek tidal stations, see Fig. 1) are smaller than 5 minutes. Values for ME_{HWL} range from -0.04 to +0.01 m near the Saeftinghe marsh.

Table 2. Comparison between observed and simulated series of tidal water levels along the estuary (see Fig. 1 for locations of the tidal stations), showing the distance from the estuary mouth (x), mean error (ME), mean absolute error (MAE) and root mean squared error (RMSE), and comparison between observed and simulated HWLs, showing the ME_{HWL} *and* $\Delta\varphi_{-HWL}$.

Tidal station	x	ME	MAE	RMSE	ME_{HWL}	$\Delta\varphi_{-HWL}$
	km	*m*	*m*	*m*	*m*	*min*
Vlissingen	2	0.02	0.05	0.06	0.07	0.2
Terneuzen	24	-0.03	0.09	0.10	0.03	-2.1
Hansweert	42	-0.06	0.09	0.12	0.01	-8.5
Baalhoek	52	-0.06	0.07	0.09	-0.04	-2.7
Bath	61	-0.05	0.08	0.10	0.01	0.8
Liefkenshoek	74	-0.06	0.10	0.13	-0.01	3.8
Antwerpen	91	-0.09	0.13	0.16	-0.04	8.4

The model performance in the Saeftinghe marsh itself is validated by a comparison between modeled and observed tidal water level series at measurement locations in the channel system and on the marsh platform (Table 3, see Fig. 2 for measurement locations). Mean errors for the full series of simulated water levels vary between -0.02 m and -0.11 m, indicating that the water levels are slightly underestimated throughout the marsh system. HWLs at the marsh edge location (loc. 8) are simulated with a ME_{HWL} of -0.03 m and phase difference of -2 minutes, which is a similar accuracy as at the nearby tidal stations in the estuary (Table 2). Halfway along the main channel (loc. 10), HWLs are represented with a ME_{HWL} and $\Delta\varphi_{-HWL}$ of +0.02 m and -1.8 min respectively. At the inner marsh locations (loc. 1, 2 and 3), situated at the end of the main channel and narrower side-channels, values for ME_{HWL} range from 0.00 m to +0.05 m and average phase differences are 3.8 and 16 minutes respectively. It should be stated that the model validation for the locations on the platform is only based on a limited number of tides (i.e., two tides at loc. 5 and six tides at loc. 6).

Table 3. Comparison between observed and simulated series of tidal water levels in the marsh (see Fig. 2 for measurement locations), including mean error (ME), mean absolute error (MAE) and root mean squared error (RMSE), and for the HWLs specifically the mean error (ME_{HWL}*) and mean phase difference (*$\Delta\varphi_{-HWL}$*).*

Measurement location		**ME**	**MAE**	**RMSE**	**ME_{HWL}**	**$\Delta\varphi_{-HWL}$**
		m	*m*	*m*	*m*	*min*
Loc. 8	*marsh edge*	-0.11	0.11	0.12	-0.03	-2.0
Loc. 10	*main channel*	-0.08	0.12	0.14	0.02	-1.8
Loc. 1	*main channel*	-0.10	0.14	0.24	0.00	-3.5
Loc. 2	*side channel*	-0.07	0.16	0.21	0.05	-3.8
Loc. 3	*side channel*	-0.10	0.13	0.19	0.01	16
Loc. 5	*platform*	-0.02	0.06	0.07	-0.01	-20
Loc. 6	*platform*	-0.05	0.06	0.08	-0.02	0.0

Water level variations during the two storm tides are fairly well represented. For the highest storm tide, during which no attenuation was present in the observations, the model results do not show any attenuation either. For the second highest storm tide, the model slightly underestimates the measured HWL reduction between locations 10 and 1 (i.e. -6.6 cm instead of -7.4 cm reduction). HWLs during the storm tides are generally underestimated throughout the domain of the model. At the study area, HWLs are underestimated by approximately 16 cm for this second highest storm tide, probably due to the absence of wind in the model schematization. During the high water slack of the highest storm tide, hourly averaged wind speeds of 8 to 11 m/s from a west- to northwest direction were present at the study area (data obtained from Royal Netherlands Meteorological Institute, http://www.knmi.nl). According to the basic formula for wind setup by Keulegan (1951), these wind speeds induce water level setup of several centimeters across the estuary channel and of around 5 cm (in WNW direction) locally in the marsh itself.

Finally, an artificial series of regular tides and storm tides (Fig. 3) is simulated to compare amplification and attenuation rates (*dHWL/dx*) for a wider range of HWLs than those of the measurements only (Fig. 4). The water level observations show a tendency of slight amplification for tides with peak water levels below the marsh platform elevation. Once the platform gets inundated, attenuation starts to occur and attenuation rates increase up to a maximum of about 5 cm/km for inundation heights around 0.5-1.0 m, after which attenuation rates decrease again. Along the inner marsh sections (i.e., loc. 10 to loc. 1 and 3), this observed relation between attenuation rates and marsh flooding depth is captured by the model (Fig. 4). In the outer marsh section (loc. 8 to loc. 10), the model predicts a slight amplification up to 1 cm/km for most tides while attenuation of up to 2 cm/km was observed. For undermarsh tides specifically, the model underestimates the observed amplification along the inner marsh sections by 1 to 4 cm/km between loc. 1 and 3. Nevertheless, the model reproduces the dependency of the amount of attenuation or amplification on the HWL relative to the platform elevation, especially for overmarsh tides (Fig. 4).

3.2 Model scenarios with varying marsh geometry and dike position

Along-channel water level variations (*dHWL/dx*) are calculated for all geomorphological scenarios described in Table 1. When the variation of HWLs along the S-, Y- and H- channel sections is considered for the reference scenario (Run 0), distinct spatial differences in HWLs arise (Fig. 5). Modeled HWLs of the 4 m storm tide increase from the marsh edge into the outer 1.5-3.0 kilometers of the S- and Y-transects and remain fairly constant along the outer part of the H-transect. Over the inner sections of the marsh channels (i.e., S3-S6, Y3-Y6, H3-H6), HWLs decrease again, resulting in a net attenuation along the full Y- and H-transects and negligible net changes along the full S-transect. Along the innermost part of the Y- and H-transects, HWLs do not decrease any further. This can be attributed to set up and reflection against the dike on the south side of the marsh (Section 3.2.1). Furthermore, scenario analyses with varying platform and channel elevation show that attenuation rates along intertidal channels vary largely with marsh geomorphology (Sections 3.2.2 and 3.2.3). In these analyses attenuation rates are only given for the inner marsh sections (i.e. S3-S6 and Y3-Y6) as the focus is on attenuation of HWLs along marsh channels, rather than on the slight amplification along the outer sections where the influence of the marsh platform is small. Finally, spatial variations in attenuation or amplification of HWLs are assessed by comparing them with local geometrical characteristics of the marsh (Section 3.3).

3.2.1 Impact of dike position and marsh size

From a comparison between the reference simulation (Run 0 in Fig. 6) and simulations in which the dike south of the marsh is repositioned and the marsh platform is extended by 1 km (Run 1 in Fig. 6) and by 5 km (Run 2 in Fig. 6), it becomes clear that attenuation rates are highly influenced by the dike position and hence the marsh size. If the dike is positioned too close to the seaward marsh edge, making the marsh extent shorter than a certain critical width (here smaller than 6 to 10 km of marshland), the highest tides and storm tides are not much attenuated or even slightly amplified (Fig. 6e and 6f). The result of the simulation with the 1 km extended platform indicates that even a small strip of additional marsh platform area can significantly improve the storm surge attenuation capacity of a marsh. While HWLs of around 1.5 m above platform elevation are not attenuated at all in the reference simulation, a platform extension of 1 km leads to maximum attenuation rates of 7 cm/km along the S3-S6 section and of over 10 cm/km along the Y3-Y6 section. Similar to the reference scenario, attenuation rates in the simulation with 1 km platform extension decrease again and turn into amplification for even higher storm tides (i.e., > 2 m above platform elevation). The results of the simulation with the 5 km extended platform do not show this strong decrease in attenuation rates for the highest HWLs. Instead, attenuation rates remain similar or appear to decrease slightly for the highest storm tides.

3.2.2 Impact of channel depth

The model results show that deeper marsh channels result in lower attenuation rates compared to the reference scenario, while shallower marsh channels lead to an increase in attenuation rates. In particular, maximum attenuation rates along the Y3-Y6 transect change from 6 cm/km for the reference simulation (Run 0 in Fig. 6b) to 4 cm/km for a simulation in which the channel elevation is lowered by 0.9 m (Run 3 in Fig. 6b) or increase to 10 cm/km for the simulation in which the channel elevation is raised by 0.7 m on average (Run 4 in Fig. 6b). Maximum attenuation rates along the S3-S6 transect are around 2.5 cm/km, 4 cm/km and 7 cm/km for the simulations with a lowered channel elevation (Run 3), the reference simulation (Run 0) and the simulation with increased channel elevation (Run 4) respectively (Fig. 6a). The general trend of increased attenuation rates for overmarsh tides up until a certain maximum and decreasing attenuation or even amplification for the highest storm tides is persistent for all scenarios with varying channel elevations.

3.2.3 Impact of platform elevation

Model results show that the elevation of the marsh platform determines the range of HWLs for which attenuation takes place (Figure 6c and 6d). In all scenarios with varying platform elevations, attenuation only occurs for overmarsh tides that inundate the marsh platform up to about 1.2 m. On the other hand, undermarsh tides with HWLs below the marsh platform elevation are not attenuated in the model results. Modeled attenuation rates are highest for overmarsh tides that are approximately 0.5 to 1.0 m above the mean marsh platform elevation. For higher tides, attenuation rates are decreasing or changing into amplification, which is shown to be the result of blockage by the dike behind the marsh area (Fig. 6e and 6f). Maximum attenuation rates are all within the range of 6.5 to 7.5 cm/km along the Y3-Y6 transect for simulations in which platform elevations have been either lowered (Run 5 in Fig. 6d) or raised (Run 6 in Fig. 6d) by 0.4m. Along the S3-S6 transect, maximum attenuation rates are lower; ranging from 3.5 to 5 cm/km.

3.3 Relations between attenuation rates and marsh geometry

For storm tides with HWLs of at least 0.4 m above mean platform elevation, a correlation can be found between the simulated attenuation rates (*dHWL/dx*) and the ratio (α_v) between the water volume on the vegetated platform and the total water volume on the marsh platform and in the channels ($r^2 = 0.92$ and $p < 0.001$, see Fig. 7):

$$(4) \qquad dHWL/dx = -36.2 * \alpha_V + 8.0$$

The relationship is based on Run 2, in which the marsh platform is extended to avoid the influence of blockage against the dikes on the modeled water level variations. Attenuation starts to occur when α_v exceeds 0.2-0.4 and increases gradually from there on. As α_v is dependent on marsh geometry and the height of the flood wave, this correlation explains both spatial variations (between marsh sections) and temporal variations (between tides with different HWLs) in attenuation rates. The highest computed attenuation rates are up to 29 cm/km over the Y5-Y6 channel section. Attenuation does not occur for any of the simulated storm tides along the outer marsh sections S1-S2-S3 and Y1-Y2-Y3. Sensitivity analyses show that the coefficients in Eq. 4 alter if the bottom friction on the marsh platform is changed. In particular, if n_v for the vegetated platform is lowered to 0.04, Eq. 4 changes to $dHWL/dx = -27.2*\alpha_V + 6.2$ ($r^2 = 0.86$ and $p < 0.001$) and the maximum modeled attenuation decreases to 23 cm/km. Conversely, if n_v increases to 0.12, Eq. 4 changes to $dHWL/dx = -41.1*\alpha_V + 9.2$ ($r^2 = 0.92$ and $p < 0.001$), while the maximum attenuation increases to 32 cm/km.

Other cross-sectional geometrical properties such as width and depth convergence length scales, channel width, the water depth in the channel or on the platform, total cross-sectional area or the ratio between water depth on the platform and in the channels could not be related to the modeled attenuation rates and are therefore not shown. Only the tide-independent ratio between the platform surface area and the total surface area of the channel and adjacent platform (α_A) can be used to explain differences in maximum attenuation rates between different channel sections (Fig. 8). Attenuation only occurs along relatively small channels where α_A is larger than 0.5. From there, maximum attenuation rates are increasing with increasing values for α_A. Conversely, amplification is persistent for all tides along channel sections with α_A below 0.5, except for the slight attenuation for some tides along the Y2-Y3 section. However, α_A does not account for variations in attenuation rates between different tides with varying HWLs.

4. Discussion

4.1 Model performance

The hydrodynamic model that is used to compute HWL attenuation rates across marshes represents observed water level variations (Stark et al., 2015) along intertidal marsh channels over a distance of several kilometers fairly well (Table 3). The model results capture the observed dependency of attenuation rates on the HWL relative to the platform elevation (Fig. 4). In particular, modeled attenuation rates increase (or amplification rates decrease) as HWLs increase above the platform elevation up until a maximum for HWLs of around 0.7-0.8 m above platform elevation, from which attenuation rates decrease (or amplification rates increase) again. The model also captures observed attenuation and amplification rates for overmarsh tides along the inner marsh sections (i.e., loc. 10 to 1 and 3) where attenuation is strongest and on which the main conclusions of this study are based. Nevertheless, some discrepancy between the model results and the observations exists. Firstly, the model underestimates observed attenuation in the outer part of the channel where slight amplification is predicted for most overmarsh tides. This suggests that bottom friction applied in the model along this section is too low to simulate the observed dampening of the tidal wave (Friedrichs and Aubrey, 1994; Van Rijn, 2011). Bottom friction along the outer part of the marsh channel could indeed be higher in reality due to the presence of coarser (sandy) sediments (Jongepier et al., 2015) and large bed forms in the outer part of the channel (Huijs, 1995), which may be the result of higher flow velocities in the deeper and wider outer channel parts as compared to the shallower and smaller inner channel parts. Results from the model calibration show that attenuation along this section increases if a higher Manning coefficient is applied. Hence, spatially varying Manning coefficients (i.e., higher in the outer than in the inner channel parts) could improve the overall model performance. However, it would reduce the generic character of our model scenarios and conclusions on the effect of marsh channel and platform geometry, as differences in attenuation rates between the scenarios could then be attributed to spatial differences in channel bed friction, instead of solely differences in marsh channel geometry and platform extent. A second discrepancy is the underestimation of observed amplification by 1 to 4 cm/km for undermarsh tides along the narrowest inner marsh section (i.e., loc. 10 to 3) by the model. This could be due to limitations in the resolution of the bathymetry data and of the mesh itself, which causes some deeper parts of the channels to be missing or smoothed out in the model bathymetry, especially affecting lower tides (i.e., due to the inverse relationship between water depth and bottom friction). Despite the above-discussed discrepancies between observed and modelled attenuation for the outer marsh sections and for undermarsh tides, we emphasize that the conclusions of our study are based on the model results for overmarsh tides along the inner marsh sections, where observations are indeed well reproduced by the model.

4.2 Effect of marsh size and dike position

One important finding of this study is that limitations in storage area or marsh extent have a considerable impact on storm surge attenuation and may drastically reduce attenuation rates (Fig. 6e and 6f). Storage area limitations can be caused by the blockage or reflection against a dike or similar structure confining the marsh surface area (Wamsley et al., 2010, 2009) and prevent a marsh from reaching its full attenuation capacity. This mechanism was hypothesized by Resio and Westerink (2008), who argued that attenuation rates decrease if the duration of the hydrodynamic forcing is long compared to the time needed to fill the available storage area. In that case, the propagating flood wave is blocked or reflected before HWLs reach the end of a basin or marsh platform, leading to higher HWLs at the landward end of the marsh and hence lower attenuation rates. Moreover, attenuation rates can even be minimized or amplification of HWLs can occur, as is the case for the highest storm tides in the reference simulation and the simulation in which the dike is moved landward by 1 km (Fig. 6). The simulation in which the platform is extended much further by 5 km does not show a drastic decrease in attenuation rates for higher overmarsh storm tides. In that simulation, the propagating peak of the tidal wave has not yet reached the dike behind the marsh before the ebb tide starts and water levels decrease again. Therefore, storage area limitations do not affect HWL reduction in the studied marsh section in this simulation. Sensitivity of storm surge reduction to limitations in storage area relative to the duration of the hydrodynamic forcing implies that the duration of a storm surge or flood wave affects storm surge reduction rates across a given wetland (Hu et al., 2015; Liu et al., 2013; Resio and Westerink, 2008). In this context it should be mentioned that only tidal waves with a more or less constant period are considered in this study. In micro-tidal cases however, faster moving storms cause flood waves with a shorter duration and are found to result in higher storm surge reduction rates than slower moving storms with longer flood wave durations (Hu et al., 2015; Liu et al., 2013; Sheng et al., 2012; Zhang et al., 2012).

Following the reasoning of Resio and Westerink (2008), we hypothesize that a minimum wetland size exists for which the attenuation capacity of the area is fully used and is not anymore affected by blockage effects against dikes of other structures behind the marsh. This minimum wetland size would depend on the duration of the flood wave and on site-specific variables that affect the landward propagation of the flood wave, such as the presence and size of channels and friction exerted by the vegetation. Based on the present model results for storm tides only, the minimum extent of the studied marsh should be between 6 and 10 km to completely avoid blockage effects for the highest modeled storm tides and to optimize the attenuation capacity of the marsh. It must be stated however that the extended part of the marsh is rather schematically implemented and does not contain any channels. In reality, a larger marsh area would yield larger channels in the existing part of the marsh due to the relation between channel size and drainage volume (D'Alpaos et al., 2010; Vandenbruwaene et al., 2015), while a channel network would develop in the extended marshland as well. The current schematization of the marsh extension could rather be seen as supra-tidal marshland. Because of these limitations in the model schematization and the dependency on event-specific variables, a general definition of this minimum wetland size cannot readily be evaluated with the present model results.

4.3 Influence of marsh geometry

The model results show that the depth of marsh channels affects the amount of HWL reduction (Fig. 6a and 6b). Deeper channels exert less friction and lead to a reduction of marsh scale attenuation rates, while shallow marsh channels exert more friction and increase marsh scale attenuation rates. Nevertheless, the model results did not reveal a distinct relationship between the water depth in the channel and the attenuation rate that holds for tides with varying HWLs. These results are consistent with findings of existing numerical studies (Loder et al., 2009; Temmerman et al., 2012) and can be explained by the inverse relationship between channel depth and bottom friction exerted on the flow. If local surge generation would be of importance, marsh channel depth could have a contrasting effect on *dHWL/dx* as surge generation decreases with increasing depth (Rego and Li, 2009; Resio and Westerink, 2008). In our study, surge generation occurs outside the model domain and surge height is incorporated as boundary condition for the model

In contrast to channel depth, the marsh platform elevation barely affects the maximum attenuation rate along marsh sections. Platform elevation is however an indicator for the range of tides that are attenuated and which tides are most heavily damped (Fig. 6c and 6d). Undermarsh tides with HWLs below marsh platform elevation and, which only flood the marsh channel network, are not attenuated or are even slightly amplified. Overmarsh tides that also inundate the vegetated marsh platform are increasingly attenuated for higher HWLs, as long as limitations in storage area are not considered. These findings are in accordance with the observations by (Stark et al., 2015) on which the model is based. Furthermore, the model results indicate that marshes with a lower platform elevation induce the highest attenuation rates for relatively low inundation events compared to marshes with a higher platform elevation (i.e., as long as the limitation in storage area due to confinement by the dikes does not affect the HWL reduction) (see Fig. 6 c/d, HWLs between 2.5 m and 3.5 m). As limitations in storage area reduce attenuation rates on the lower marsh for increasing HWLs, the higher marsh becomes more effective. If the platform elevation is higher, blockage effects only start to affect attenuation rates for higher HWLs. This can be attributed to slower flood wave propagation on higher marsh platforms due to smaller water depths. A greater effectiveness of high marshes in a confined system was also found by Wamsley et al. (2009). Moreover, Loder et al. (2009) found that for high platform elevations smaller surge events are generally attenuated, while larger surge events are amplified. Our results are consistent with these findings and show as well that decreased attenuation rates or amplification for larger surge events can be due to set up against dikes confining the marsh, especially if such larger surge events have a longer duration.

4.4 Relationship between marsh geometry, peak water levels and attenuation rates

As attenuation rates vary temporally between flood events and spatially between marsh sections, parameters solely based on marsh geometry, such as the ratio α_A between platform surface area and total surface area, can only explain spatial variations in attenuation rates for single flood events. However, they do not explain variations in attenuation rates between tides with different HWLs (Fig. 8), implying that a tide-varying parameter is needed. The present model results provide for a relation between along channel variations in HWLs and the tide-varying ratio α_v between water volume on the vegetated platform and the total water volume (Eq. 4). This relationship combines geometrical and hydrodynamic variations (both present in α_v) to explain differences in attenuation rates. The relationship applies only to a situation without confinement by dikes or other structures, as it is based on the model simulation with the extended marsh platform (i.e., Run 2 in Table 1). Moreover, we assume that large-scale sheet flow occurs over the marsh platform, implying that flow routing through the channel network does not affect attenuation rates. Previous studies showed that this is the case for tides with HWLs above the canopy height of the vegetation (Temmerman et al., 2005a, 2005b; Vandenbruwaene et al., 2015), which is around 0.4 m for the most abundant species in our study area. Although the vegetation stem height is not explicitly implemented in the model, Eq. 4 is also based on storm tides with HWLs that are at least 0.4 m above the mean platform elevation for which sheet flow over the marsh platform actually occurs in the model simulations. The coefficients in the Eq. 4 are likely to vary with site-specific parameters such as vegetation-type and bottom roughness. In this study, a constant Manning's *n* coefficient of 0.08 is used to implement the additional friction and drag force exerted by the marsh vegetation. More dense vegetation such as mangrove forests would exert higher friction and drag forces on the flow, leading to higher attenuation rates (e.g., Krauss et al., 2009) and hence a different relationship between α_v and *dHWL/dx*. A sensitivity analysis with model simulations in which the Manning coefficient of the vegetated marsh platform is altered indicates that Eq. 4 indeed varies for different friction coefficients. The flood wave period will also affect attenuation rates (e.g., Sheng et al., 2012; Zhang et al., 2012) and hence the relationship described above. Hypothetically, similar relationships could be found for different wetland types (i.e., different friction coefficients) and for flood waves with a different duration, ranging from tidal inundation events as described in this study to long flood waves caused by large cyclones or hurricanes. Further research is necessary to test this hypothesis and possibly find relationships between attenuation rates, HWLs and marsh geometry for various wetland types and storm surge durations. Nonetheless, the present model results are potentially applicable to attenuation of storm tides in other marshes with similar characteristics (i.e., macrotidal marshes which are dominated by flexible wetland grasses). In reality, marsh channel and platform elevations may vary between marsh sites (due to differences in tidal range or sediment availability) or may change over time (due to long-term morphological development or changing hydrodynamic conditions). Our model scenarios with varying marsh size and different marsh channel and platform elevations contribute to fundamental insights on how flood attenuation rates vary with such space- and time-dependent marsh geomorphological properties. Therefore, the presented results are of interest to coastal managers that want to implement wetlands or marshes as part of their coastal defense structures or coastal managers and scientists who want to examine the coastal defense capacity of existing marshes.

Acknowledgements

The authors would like to thank the Port of Antwerp for funding this research. Furthermore, we thank CalcUA for their assistance and usage of their HPC infrastructure.

References

Barbier, E.B., 2014. A global strategy for protecting vulnerable coastal populations. Science 345, 1250–1251. doi:10.1126/science.1254629

Cheong, S.-M., Silliman, B., Wong, P.P., van Wesenbeeck, B., Kim, C.-K., Guannel, G., 2013. Coastal adaptation with ecological engineering. Nat. Clim. Chang. 3, 787–791. doi:10.1038/nclimate1854

D'Alpaos, A., Lanzoni, S., Marani, M., Rinaldo, A., 2010. On the tidal prism-channel area relations. J. Geophys. Res. Earth Surf. 115, 1–13. doi:10.1029/2008JF001243

Friedrichs, C.T., Aubrey, D.G., 1994. Tidal propagation in strongly convergent channels. J. Geophys. Res. 99, 3321–3336. doi:10.1029/93JC03219

Gedan, K.B., Kirwan, M.L., Wolanski, E., Barbier, E.B., Silliman, B.R., 2010. The present and future role of coastal wetland vegetation in protecting shorelines: Answering recent challenges to the paradigm. Clim. Change 106, 7–29. doi:10.1007/s10584-010-0003-7

Hervouet, J.-M., 2007. Hydrodynamics of Free Surface Flows: Modelling with the finite element method. doi:10.1002/9780470319628

Hinkel, J., Lincke, D., Vafeidis, A.T., Perrette, M., Nicholls, R.J., Tol, R.S.J., Marzeion, B., Fettweis, X., Ionescu, C., Levermann, A., 2014. Coastal flood damage and adaptation costs under 21st century sea-level rise. Proc. Natl. Acad. Sci. U. S. A. 111, 3292–7. doi:10.1073/pnas.1222469111

Hu, K., Chen, Q., Wang, H., 2015. A numerical study of vegetation impact on reducing storm surge by wetlands in a semi-enclosed estuary. Coast. Eng. 95, 66–76. doi:10.1016/j.coastaleng.2014.09.008

Huijs, S., 1995. Geomorfologische ontwikkeling van het intergetijdegebied in de Westerschelde

1935-1989. Middelburg, The Netherlands.

Jones, H.P., Hole, D.G., Zavaleta, E.S., 2012. Harnessing nature to help people adapt to climate change. Nat. Clim. Chang. 2, 504–509. doi:10.1038/nclimate1463

Jongepier, I., Wang, C., Missiaen, T., Soens, T., Temmerman, S., 2015. Intertidal landscape response time to dike breaching and stepwise re-embankment: A combined historical and geomorphological study. Geomorphology 236, 64–78. doi:10.1016/j.geomorph.2015.02.012

Krauss, K.W., Doyle, T.W., Doyle, T.J., Swarzenski, C.M., From, A.S., Day, R.H., Conner, W.H., 2009. Water level observations in mangrove swamps during two hurricanes in Florida. Wetlands 29, 142–149. doi:10.1672/07-232.1

Kundzewicz, Z.W., Kanae, S., Seneviratne, S.I., Handmer, J., Nicholls, N., Peduzzi, P., Mechler, R., Bouwer, L.M., Arnell, N., Mach, K., Muir-Wood, R., Brakenridge, G.R., Kron, W., Benito, G., Honda, Y., Takahashi, K., Sherstyukov, B., 2014. Flood risk and climate change: global and regional perspectives. Hydrol. Sci. J. 59, 1–28. doi:10.1080/02626667.2013.857411

Liu, H., Zhang, K., Li, Y., Xie, L., 2013. Numerical study of the sensitivity of mangroves in reducing storm surge and flooding to hurricane characteristics in southern Florida. Cont. Shelf Res. 64, 51–65. doi:10.1016/j.csr.2013.05.015

Loder, N.M., Irish, J.L., Cialone, M.A., Wamsley, T.V., 2009. Sensitivity of hurricane surge to morphological parameters of coastal wetlands. Estuar. Coast. Shelf Sci. 84, 625–636. doi:10.1016/j.ecss.2009.07.036

Lovelace, J.K., 1994. Storm-tide elevations produced by Hurricane Andrew along the Louisiana coast, August 25-27, 1992. Open File Report 94-371. Baton Rouge, LA, U.S.

McGee, B.B.D., Goree, B.B., Tollett, R.W., Woodward, B.K., Kress, W.H., 2006. Hurricane Rita Surge Data, Southwestern Louisiana and Southeastern Texas, September to November 2005. U.S. Geological Survey Data Series 220.

McIvor, A., Spencer, T., Möller, I., Spalding, M., 2012. Storm surge reduction by mangroves. Natural Coastal Protection Series: Report 2, Cambridge Coastal Research Unit Working Paper 41.

Möller, I., Kudella, M., Rupprecht, F., Spencer, T., Paul, M., van Wesenbeeck, B.K., Wolters, G., Jensen, K., Bouma, T.J., Miranda-Lange, M., Schimmels, S., 2014. Wave attenuation over coastal salt marshes under storm surge conditions. Nat. Geosci. 7, 727–731. doi:10.1038/ngeo2251

Möller, I., Spencer, T., French, Leggett, D., Dixon, M., 1999. Wave transformation over salt marshes: A field and numerical modelling study from north Norfolk, England. Estuar. Coast. Mar. Sci. 49, 411–426. doi:10.1006/ecss.1999.0509

Nicholls, R.J., Cazenave, A., 2010. Sea-level rise and its impact on coastal zones. Science 328, 1517–1520. doi:10.1126/science.1185782

Rego, J.L., Li, C., 2009. On the importance of the forward speed of hurricanes in storm surge forecasting: A numerical study. Geophys. Res. Lett. 36. doi:10.1029/2008GL036953

Reitsma, J.M., 2006. Vegetatiekartering van de Westerschelde 2004-2005 op basis van false colour-luchtfoto's 1:5000 / 1:10.000. Delft, The Netherlands.

Resio, D.T., Westerink, J.J., 2008. Modeling the physics of storm surges. Phys. Today 61, 33–38. doi:10.1063/1.2982120

Sheng, Y.P., Lapetina, A., Ma, G., 2012. The reduction of storm surge by vegetation canopies: Three-dimensional simulations. Geophys. Res. Lett. 39, 1–5. doi:10.1029/2012GL053577

Shepard, C.C., Crain, C.M., Beck, M.W., 2011. The protective role of coastal marshes: a systematic review and meta-analysis. PLoS One 6, e27374. doi:10.1371/journal.pone.0027374

Smolders, S., Plancke, Y., Ides, S., Meire, P., Temmerman, S., 2015. Role of intertidal wetlands for tidal and storm tide attenuation along a confined estuary: a model study. Nat. Hazards Earth Syst. Sci. Discuss. 3, 3181–3224. doi:10.5194/nhessd-3-3181-2015

Stark, J., Van Oyen, T., Meire, P., Temmerman, S., 2015. Observations of tidal and storm surge attenuation in a large tidal marsh. Limnol. Oceanogr. 60, 1371–1381. doi:10.1002/lno.10104

Sutton-Grier, A.E., Wowk, K., Bamford, H., 2015. Future of our coasts: The potential for natural and hybrid infrastructure to enhance the resilience of our coastal communities, economies and ecosystems. Environ. Sci. Policy 51, 137–148. doi:10.1016/j.envsci.2015.04.006

Temmerman, S., Bouma, T.J., Govers, G., Lauwaet, D., 2005a. Flow paths of water and sediment in a tidal marsh: Relations with marsh developmental stage and tidal inundation height.

Estuaries 28, 338–352. doi:10.1007/BF02693917

Temmerman, S., Bouma, T.J., Govers, G., Wang, Z.B., De Vries, M.B., Herman, P.M.J., 2005b. Impact of vegetation on flow routing and sedimentation patterns: Three-dimensional modeling for a tidal marsh. J. Geophys. Res. 110, F04019. doi:10.1029/2005JF000301

Temmerman, S., De Vries, M.B., Bouma, T.J., 2012. Coastal marsh die-off and reduced attenuation of coastal floods: A model analysis. Glob. Planet. Change 92-93, 267–274. doi:10.1016/j.gloplacha.2012.06.001

Temmerman, S., Kirwan, M.L., 2015. Building land with a rising sea. Science 349, 588–589. doi:10.1126/science.aac8312

Temmerman, S., Meire, P., Bouma, T.J., Herman, P.M.J., Ysebaert, T., De Vriend, H.J., 2013. Ecosystem-based coastal defence in the face of global change. Nature 504, 79–83. doi:10.1038/nature12859

Van der Molen, J., 1997. Tidal distortion and spatial differences in surface flooding characteristics in a salt marsh: Implications for sea-level reconstruction. Estuar. Coast. Shelf Sci. 45, 221–233. doi:10.1006/ecss.1997.0179

Van Rijn, L.C., 2011. Analytical and numerical analysis of tides and salinities in estuaries; part I: tidal wave propagation in convergent estuaries. Ocean Dyn. 61, 1719–1741. doi:10.1007/s10236-011-0453-0

Vandenbruwaene, W., Schwarz, C., Bouma, T.J., Meire, P., Temmerman, S., 2015. Landscape-scale flow patterns over a vegetated tidal marsh and an unvegetated tidal flat: implications for the landform properties of the intertidal floodplain. Geomorphology 231, 40–52. doi:10.1016/j.geomorph.2014.11.020

Vanlierde, E., Ferket, B., Michielsen, S., Vereycken, K., Van Hoestenberghe, T., Levy, Y., Plancke, Y., Deschamps, M., Verwaest, T., Mostaert, F., 2014. MONEOS - jaarboek monitoring WL 2013: Factual data rapportage van monitoring hydrodynamiek en fysische parameters zoals gemeten door WL in het Zeescheldebekken in 2013. Versie 4.0. WL Rapporten, 12_070. Antwerpen.

Wamsley, T. V., Cialone, M. a., Smith, J.M., Atkinson, J.H., Rosati, J.D., 2010. The potential of wetlands in reducing storm surge. Ocean Eng. 37, 59–68.

doi:10.1016/j.oceaneng.2009.07.018

Wamsley, T. V., Cialone, M. a., Smith, J.M., Ebersole, B. a., Grzegorzewski, A.S., 2009. Influence of landscape restoration and degradation on storm surge and waves in Southern Louisiana. Nat. Hazards 51, 207–224. doi:10.1007/s11069-009-9378-z

Wang, C., Temmerman, S., 2013. Does biogeomorphic feedback lead to abrupt shifts between alternative landscape states?: An empirical study on intertidal fl ats and marshes. J. Geophys. Res. 118, 229–240. doi:10.1029/2012JF002474

Weisberg, R., Zheng, L., 2006. Hurricane Storm Surge Simulations for Tampa Bay. Estuaries and Coasts 29, 899–913. doi:10.1007/BF02798649

Woodruff, J.D., Irish, J.L., Camargo, S.J., 2013. Coastal flooding by tropical cyclones and sea-level rise. Nature 504, 44–52. doi:10.1038/nature12855

Zhang, K., Liu, H., Li, Y., Xu, H., Shen, J., Rhome, J., Smith, T.J., 2012. The role of mangroves in attenuating storm surges. Estuar. Coast. Shelf Sci. 102-103, 11–23. doi:10.1016/j.ecss.2012.02.021

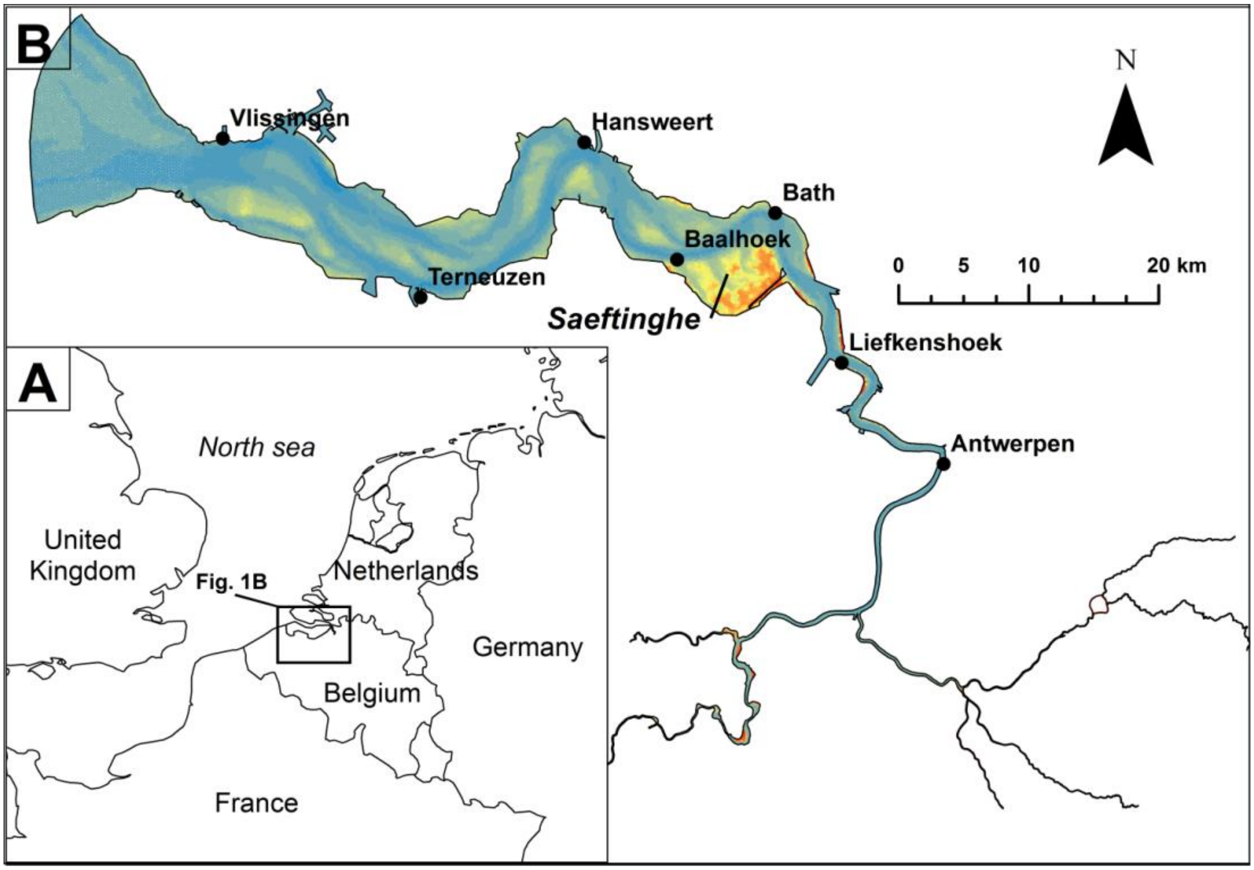

Figure 1: (a) Location of the Scheldt Estuary in Europe and (b) the Scheldt Estuary with its intertidal areas, including the tidal stations that are used in the model validation.

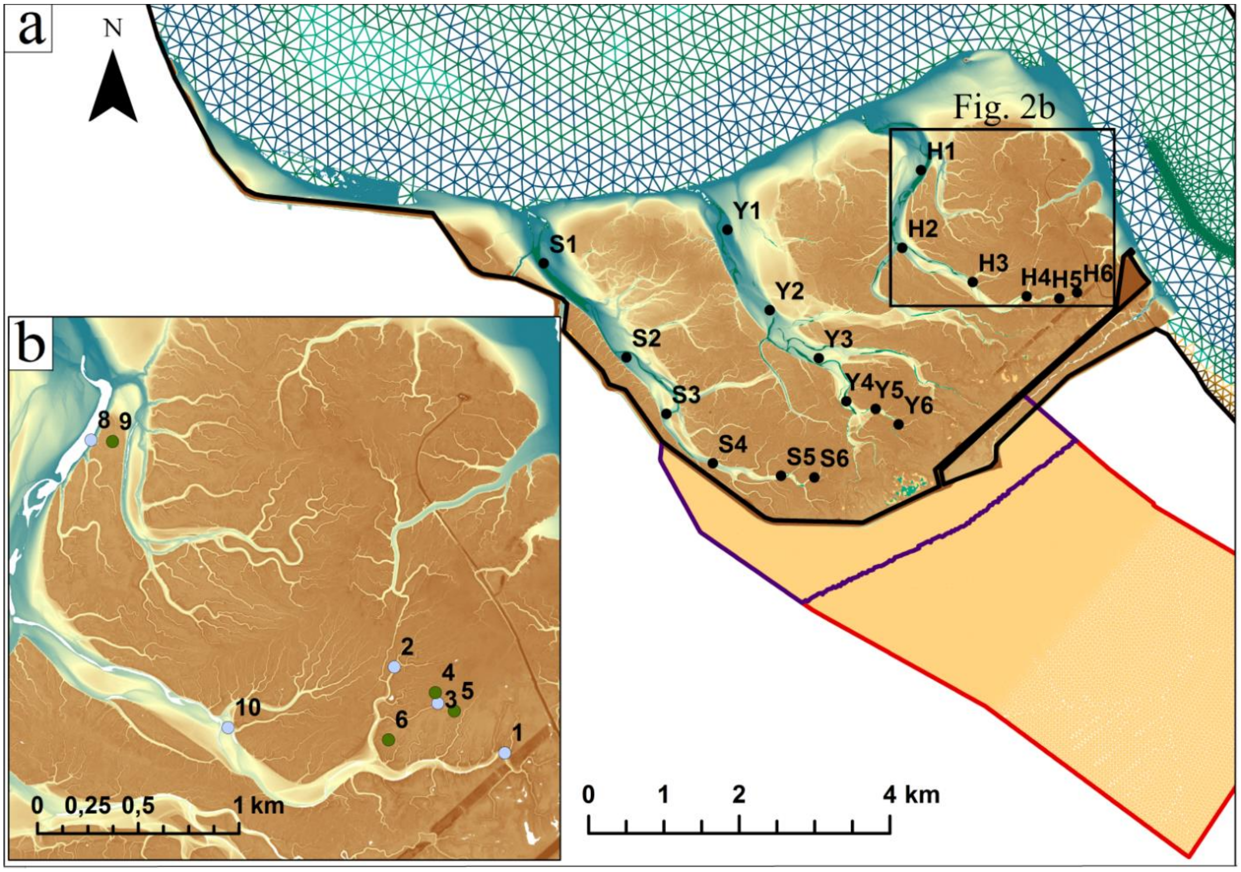

Figure 2. Saeftinghe marsh with (a) the locations along the S-, Y- and H-transects, the present dikes and model boundary (bold black line) and the model boundary for the scenarios with 1 km (purple line) and 5 km (red line) marsh platform extensions and (b) the locations of the water level observations in the channels (blue dots) and on the platform (green dots).

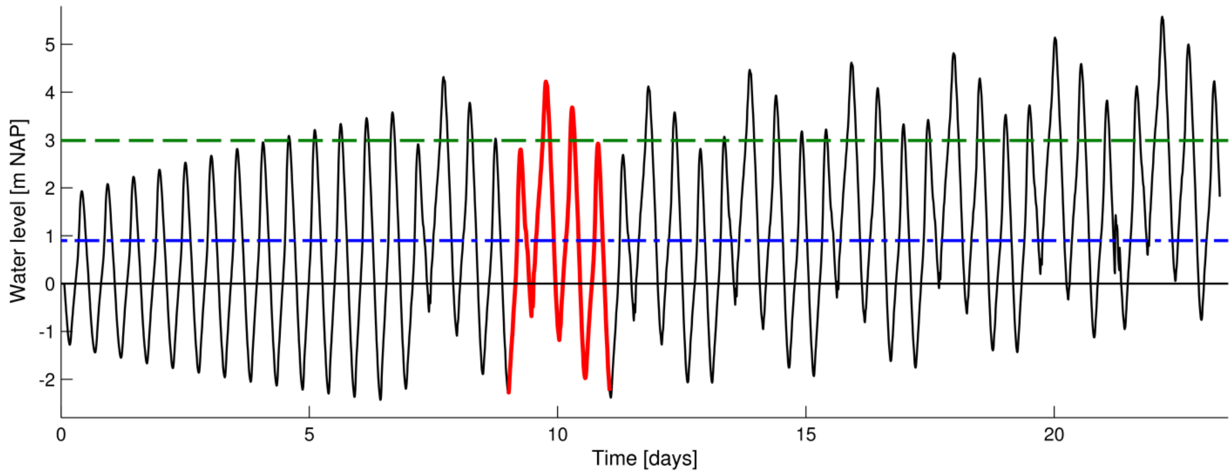

Figure 3. Modeled water level series near the study area. The measured storm tide is indicated by the red bold part. The mean platform elevation is indicated with the green dashed line and the mean elevation of the bare channels is indicated with the blue dot-dashed line.

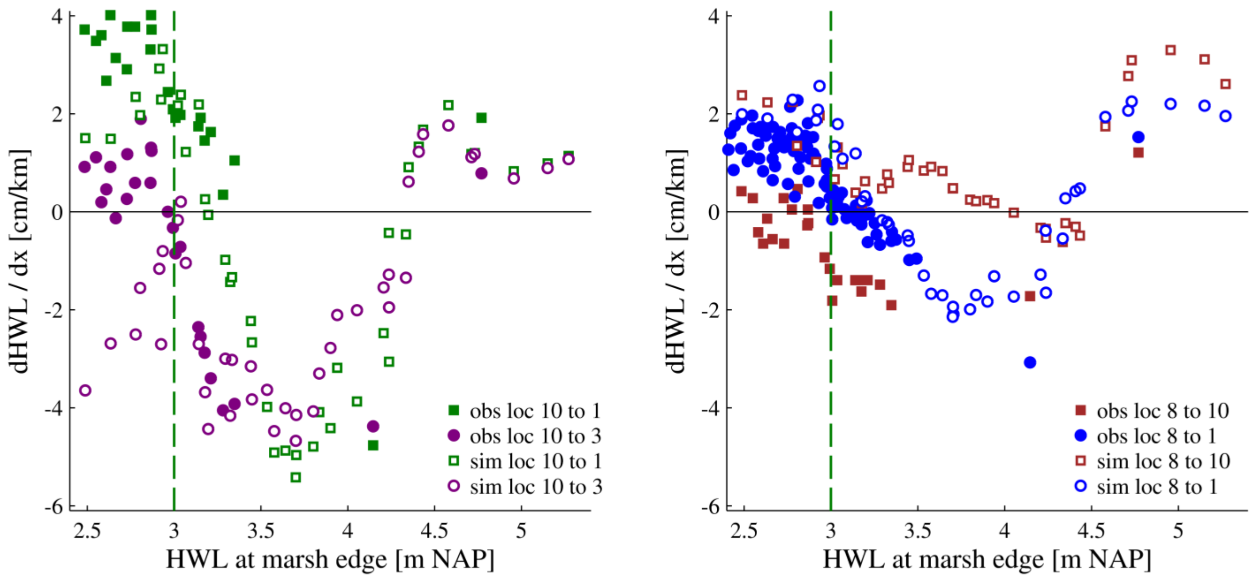

Figure 4. Observed (full markers) and modeled (open markers) attenuation and amplification rates from locations 10 to 3 (purple), 10 to 1 (green) (left graph) and 8 to 10 (brown) and 8 to 1 (blue) (right graph). The mean platform elevation is indicated by a dashed vertical green line.

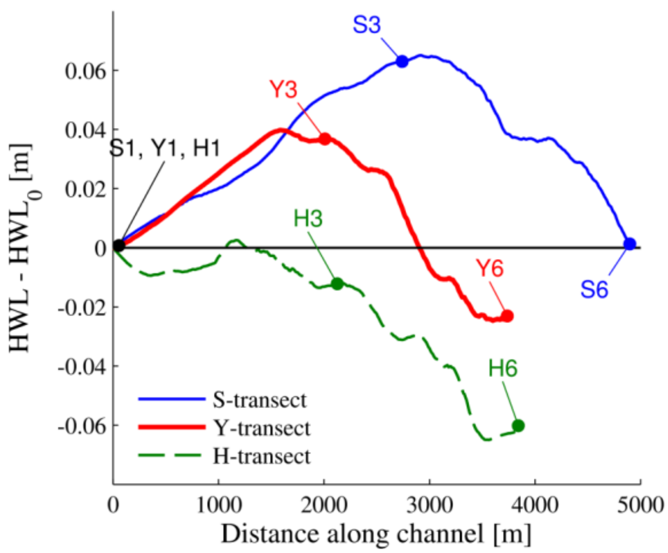

Figure 5. Variation in HWLs for a NAP +4.0 m storm tide along the S-, Y- and H-transects based on the reference scenario (Run 0). The distance along the channel is given from S1, Y1 and H1 respectively. HWLs are computed relative to the high water level at these marsh edge locations (HWL_0).

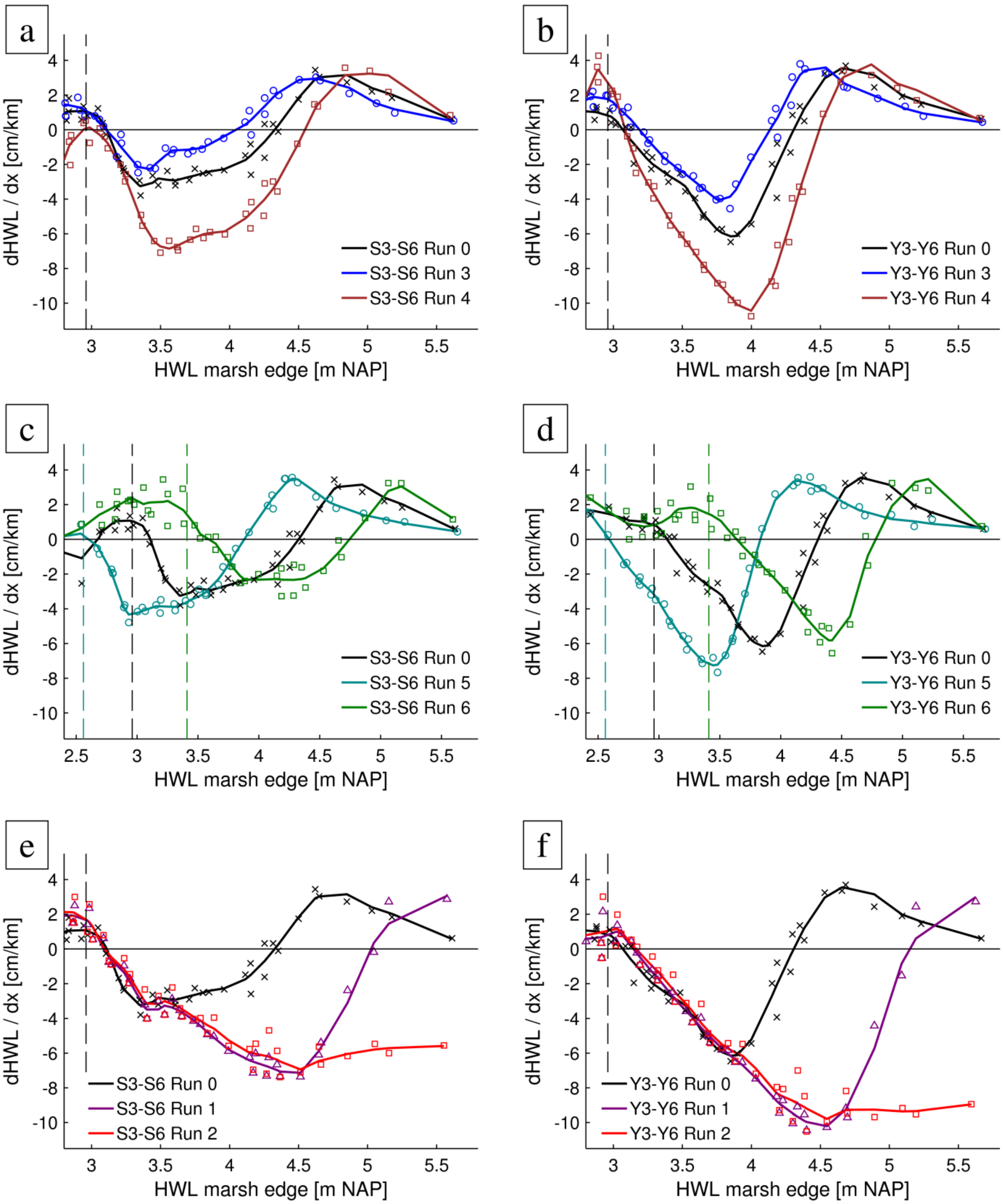

Figure 6. Modeled attenuation and amplification rates of tides with different high water levels for scenarios in which the channel elevation is varied (top), scenarios in which the platform elevation is varied (mid) and scenarios in which the dike is moved landward and the marsh

platform is extended by 1 km or 5 km (bottom) over the S3-S6 (left) and Y3-Y6 transect (right) (see Fig. 2 for transect locations). The model scenarios are explained in Table 1. Each marker represents an individual tide and the lines represent the moving average. The mean platform elevations for the different scenarios are indicated with dashed vertical lines.

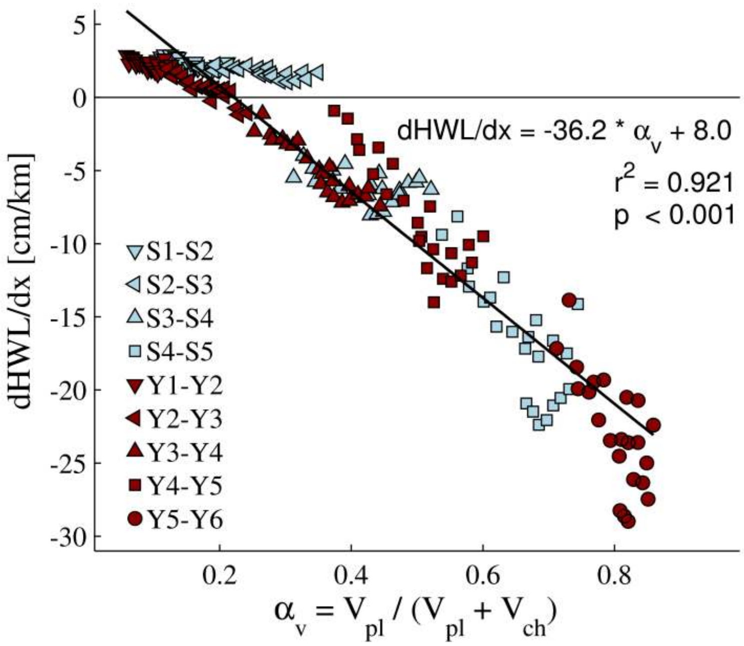

Figure 7. HWL reduction rates along channel sections in the S- (light blue) and Y- (dark red) transect for Run 2 plotted against the ratio between water volume above the platform and the total water volume (α_v). These water volumes are computed above the vegetated and non-vegetated surface areas in a strip of 500 m around each channel section.

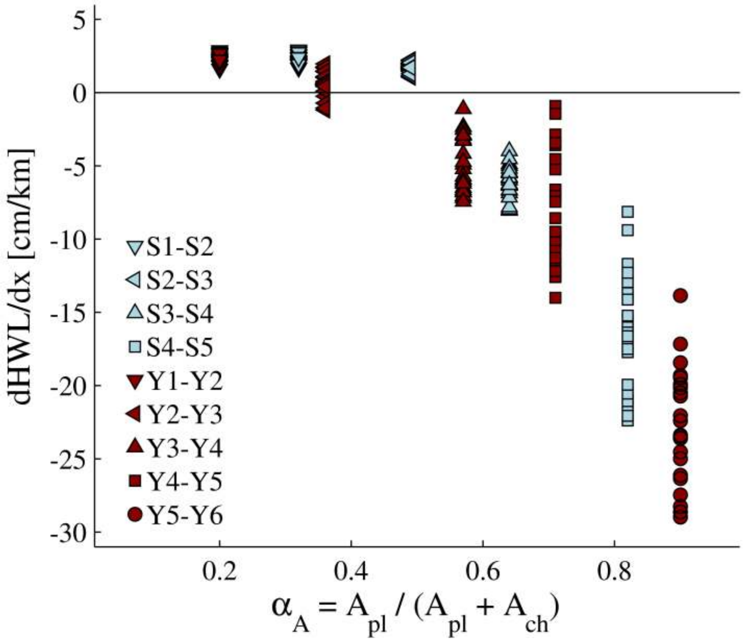

Figure 8. HWL reduction rates along the S- (light blue) and Y- (dark red) transects for Run 2 plotted against the ratio between platform surface area and total surface area (α_A), calculated based on the vegetated and non-vegetated surface area in a strip of 500 m around each channel section.